Multiscale simulations identify origins of differential carbapenem hydrolysis by the OXA-48 β-lactamase

Viivi H. A. Hirvonen[a,b,†] *, Tal Moshe Weizmann*[a,‡] *, Adrian J. Mulholland*[b]*, James Spencer*[c] *and Marc W. van der Kamp*[a,b]*

[a] School of Biochemistry, University of Bristol, University Walk, Bristol, BS8 1TD, UK; marc.vanderkamp@bristol.ac.uk, Tel: +44 117 331 2147, Fax: +44 17 331 2168.

[b] Centre for Computational Chemistry, School of Chemistry, University of Bristol, Cantock's Close, Bristol, BS8 1TS, UK.

[c] School of Cellular and Molecular Medicine, University of Bristol, University Walk, Bristol, BS8 1TD, UK.

[†, ‡] Present address listed in Author Information

KEYWORDS Antibiotic resistance, OXA-48, β-lactamase, carbapenem, QM/MM

ABSTRACT OXA-48 β-lactamases are frequently encountered in bacterial infections caused by carbapenem-resistant Gram-negative bacteria. Due to the importance of carbapenems in treatment of healthcare-associated infections, and the increasingly wide dissemination of OXA-48-like enzymes on plasmids, these β-lactamases are of high clinical significance. Notably, OXA-48 hydrolyses imipenem more efficiently than other commonly used carbapenems, such as meropenem. Here, we use extensive multi-scale simulations of imipenem and meropenem hydrolysis by OXA-48 to dissect the dynamics and to explore differences in reactivity of the possible conformational substates of the respective acylenzymes. QM/MM simulations of the deacylation reaction for both substrates demonstrate that deacylation is favoured when the 6α-hydroxyethyl group is able to hydrogen bond to the water molecule responsible for deacylation, but disfavoured by increasing hydration of either oxygen of the carboxylated Lys73 general base. Differences in free energy barriers calculated from the QM/MM simulations correlate well with the experimentally observed differences in hydrolytic efficiency between meropenem and imipenem. We conclude that the impaired breakdown of meropenem, compared to imipenem, which arises from a subtle change in the hydrogen bonding pattern between the deacylating water molecule and the antibiotic, is most likely induced by the meropenem 1β-methyl group. In addition to increased insights into carbapenem breakdown by OXA β-lactamases, which may aid design of new antibiotics or inhibitors, our approach exemplifies the combined use of atomistic simulations in determining the possible different enzyme-substrate substates, and their influence on enzyme reaction kinetics.

Introduction

The World Health organization describes antibiotic resistance as "...one of the biggest threats to global health, food security, and development today."[1] Antibiotic resistance arises naturally and evolved long ago,[2] but its emergence and dissemination have been considerably accelerated by the current excessive use of antibacterial drugs.[3, 4] This evolving resistance not only complicates standard medical practices, but also has additional expensive implications e.g. for the global economy and food production.[5-7] Moreover, we are currently living in the so-called antibiotic discovery void[8] where discovering new and safe antibacterials, especially for Gram-negative bacteria, is difficult, time-consuming, and often unprofitable for big pharmaceutical companies.[9, 10] β-Lactam antibiotics offer broad-spectrum antibacterial activity against Gram-negative bacteria and remain the most prescribed drugs in clinical practice.[11] The importance of β-lactams in healthcare has been highlighted by the World Health Organization, which includes multiple different β-lactam antibiotics in their Model List of Essential Medicine.[12] All of these antibiotics contain a four-membered β-lactam ring, which ensures antibiotic binding to penicillin-binding proteins and consequently inhibition of bacterial cell wall biosynthesis.[13, 14] Clinically used β-lactam compounds can be divided into four different groups: penicillins, cephalosporins, carbapenems, and monobactams, of which carbapenems play a critical role as potent antibiotics reserved for the most serious Gram-negative infections where alternatives are limited.[15]

Emerging resistance against β-lactams is evident, and especially in Gram-negative bacteria, β-lactamase enzymes are the main resistance mechanism against these drugs.[16] β-Lactamases block antibiotic action by hydrolysing the β-lactam ring, which impairs efficient antibiotic binding to their ultimate target in cells. The Ambler sequence-based classification divides β-lactamases into

four major subgroups: serine-β-lactamases (SBLs) comprising classes A, C, and D; and metallo-β-lactamases (MBLs), class B.[17] The hydrolysis mechanism differs between SBLs and MBLs, as SBLs utilise a nucleophilic serine residue and MBLs employ zinc cofactors.[16] Class D SBLs are referred to as OXA (oxacillinase) enzymes, stemming from their activity against the isoxazolyl penicillin oxacillin,[18] and they are currently of interest due to their wide distribution and the ability of many members of the group to inactivate carbapenems. The OXA enzymes include five subgroups of recognised carbapenemases: the OXA-23, OXA24/40, OXA-51, and OXA-58 β-lactamases are mainly found in *Acinetobacter baumannii*, while OXA-48-like β-lactamases are mostly encountered in *Enterobacterales*.[19]

In *Enterobacterales,* OXA-48 β-lactamases are among the most commonly present carbapenemases in clinical samples.[20] Their activity is relatively specific towards imipenem, but other carbapenem substrates (such as meropenem and ertapenem) are also hydrolysed, albeit slowly.[21] The specific origin of this imipenemase activity is not well established, even though variations in measured hydrolysis rates between point variants of OXA-48 hint at structural moieties contributing to specific hydrolytic phenotypes. In OXA-163, a partial deletion of the β5-β6 loop (Arg214-Pro217) and one amino acid substitution (Ser212Asp) expands the hydrolysis profile to accommodate expanded-spectrum oxyimino cephalosporins (such as ceftazidime) at the expense of efficient imipenem breakdown.[22] Further studies show that the β5-β6 loop plays a role in acquired carbapenemase activity, as engineering the OXA-48 β5-β6 loop into the non-carbapenemase OXA-10 enhances its carbapenemase activity.[23] Conversely, replacing the β5-β6 loop in OXA-48 with that of OXA-18 also alters the measured carbapenemase activity (lower k_{cat} values).[24] Site-directed mutagenesis studies of OXA-48 variants indicate that residue 214 (arginine in the wildtype OXA-48) is essential for efficient carbapenem hydrolysis.[25] In recent years,

structural studies have yielded a variety of crystal structures of OXA-48 in complex with carbapenems, which shed new light on the acylenzyme (AC) intermediate state.[26-30] Intriguingly, although the β5-β6 loop is suggested to influence carbapenem activity, the only interaction observed between the substrate and residues within this loop (Thr213-Lys218) is a water-mediated contact between the imipenem 6α-hydroxyethyl hydroxyl and Thr213.[27, 30] Furthermore, bound carbapenem tail groups (C2 substituents) seem to be dynamic and able to adopt multiple conformations, which suggests they do not form strong, specific interactions with the enzyme active site.[29]

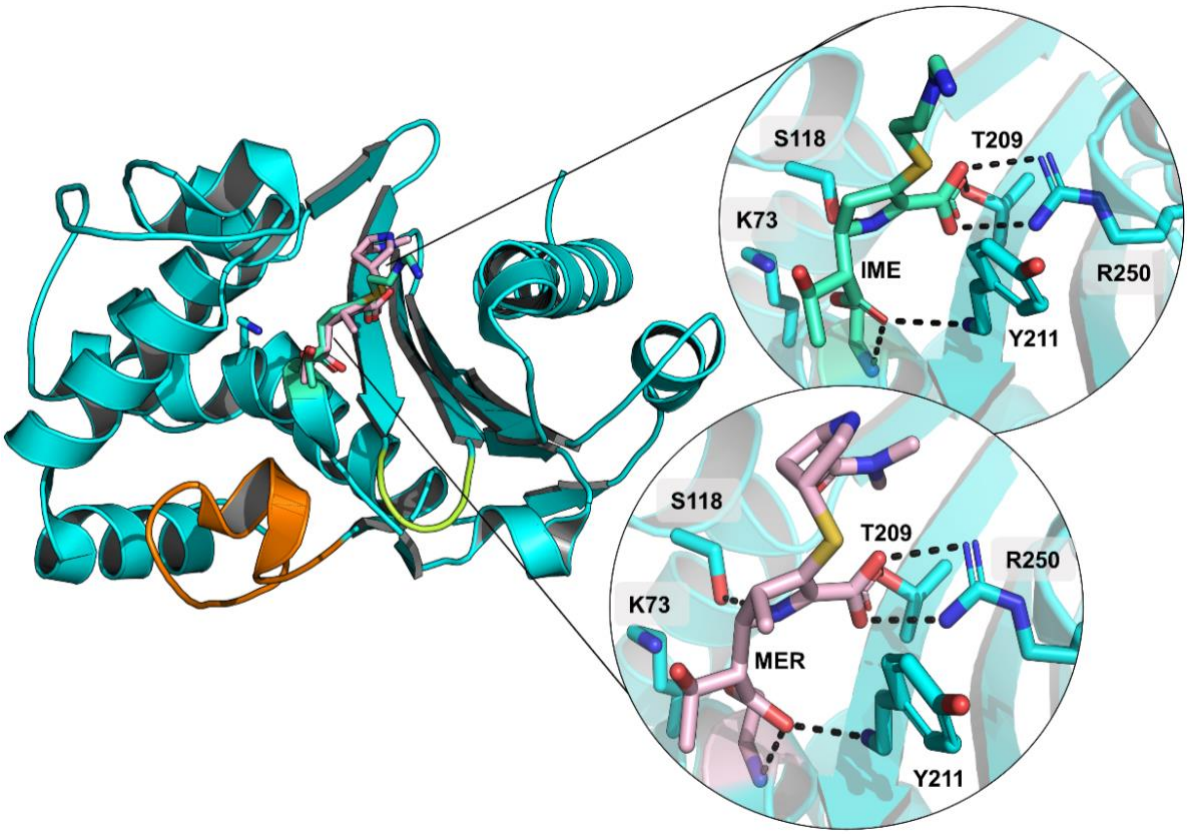

Figure 1. Crystal structures of OXA-48 complexed with carbapenems. Acylenzyme structures of OXA-48 with imipenem (PDB ID 6P97, green sticks) and meropenem (PDB ID 6P98, light pink sticks) show a very similar binding pose for both substrates, where main differences lie in the orientation of carbapenem C2 "tail" group.[27] The Ω-loop is highlighted in orange, the β5-β6-loop in yellow, and relevant active site interactions with dashed black lines. The carbapenem pyrroline ring is modelled as the Δ2-tautomer in both structures.

The generalised β-lactam hydrolysis mechanism for SBLs consists of acylation followed by deacylation.[16] Both acylation and deacylation reactions include the formation of a short-lived tetrahedral intermediate (TI) through a nucleophilic attack; the respective TI species collapses to yield either a covalent AC structure (after acylation), or the final hydrolysed product (after deacylation). In both reactions, the nucleophile (conserved serine (Ser70) in acylation and a water molecule (deacylating water, DW) in deacylation) is activated via proton abstraction by a general base. For OXA enzymes, this general base is a carboxylated lysine residue (Lys73).[31, 32] Notably, Lys73 needs to be carboxylated for optimal activity; this carboxylation is reversible and pH dependent, i.e. more carboxylation is observed at higher pH values.[31] For carbapenems, the pyrroline ring can undergo Δ2 → Δ1 tautomerization in the AC state, the Δ1 tautomer also having two stereoisomers (*R* and *S*). For class A SBLs, the Δ2 tautomer has been suggested to be the catalytically competent form, whereas the Δ1 form would essentially inhibit the enzyme.[33] For OXA-48 enzymes, all three tautomers have been observed in AC crystal structures,[27-30] but, based on NMR studies, the hydrolysis product is suggested to be either the Δ2 or *R*-Δ1 tautomer.[34]

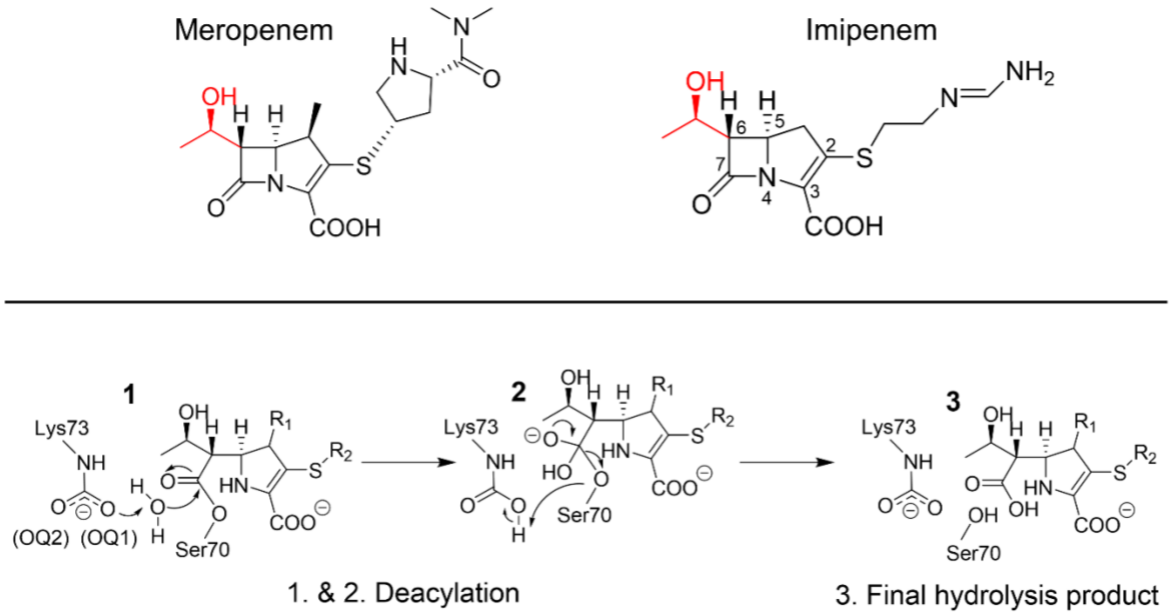

Scheme 1. Top: Structures of meropenem and imipenem (with atoms numbered), the 6α-hydroxyethyl group is highlighted in red. Bottom: Deacylation mechanism in OXA-48 with a carbapenem substrate (Δ2 tautomer). Starting from the acylenzyme, the antibiotic is deacylated via tetrahedral intermediate formation (1 → 2), which collapses to yield the hydrolysed antibiotic (3).

Kinetic measurements suggest that for OXA-48-like β-lactamases, deacylation is the rate-limiting step in carbapenem breakdown.[30] These authors suggested that the impaired imipenemase activity in the ESBL-like OXA-163, compared to OXA-48, is due to a larger active site, which would not constrain the substrate in deacylation-compatible conformations. Molecular dynamics simulations of the non-covalent complexes of OXA-48 and OXA-163 with meropenem and imipenem suggested some differences between the substrates in mobility. However, the measured K_M values for OXA-48 with imipenem and meropenem are very similar (according to one assay, 11 and 13 μM, respectively)[21], which indicates that there is unlikely to be any significant difference in the stabilities of the respective Michaelis complexes. The difference in the inactivation efficiency of imipenem compared to meropenem is thus primarily related to differences in the rate of the deacylation step, and it is therefore essential to consider this reaction when seeking to understand and explain activity differences. To analyse differences in activity for carbapenems in

atomistic detail, we here simulate TI formation in deacylation, i.e. the expected rate-limiting step, of both imipenem and meropenem by OXA-48 using combined quantum mechanics/molecular mechanics (QM/MM) simulations. Our simulations support the hypothesis that the AC state arising from carbabenem acylation is dynamic in nature. Further, we identify conformations of the 6α-hydroxyethyl group that allow for efficient deacylation. Additionally, active site hydration around the carboxylated Lys73 is observed to affect the calculated free energy barriers for deacylation, as we previously observed hydrolysis of the expanded-spectrum oxyimino cephalosporin ceftazidime by OXA-48 enzymes.[35] Analysis of the reaction simulations shows that efficient carbapenem breakdown results both from decreased hydration around carboxy-Lys73, and from subtle changes in hydrogen bonding between the substrate and the catalytic water molecule. These results provide detailed insight into the causes of differences in enzyme activity against different antibiotics, information potentially useful in understanding and combating antimicrobial resistance.

Methods

Computational methods and details of the system setup are described in detail in the Supporting Information (SI). To summarise, models of OXA-48 with imipenem and meropenem were prepared based on corresponding acylenzyme (AC) crystal structures (PDB IDs 6P97[27] and 6P98[27] for imipenem and meropenem, respectively). The ff14SB parameter set was used for the protein,[36] parameters and partial charges for non-standard residues (acylated carbapenems and carboxylated lysine) were derived with the R.E.D. Server.[37] Both systems were energy minimised, heated from 50 K to 300 K (in 20 ps), and their dynamics in the AC state were simulated for 200 ns using Langevin dynamics (collision frequency 0.2 ps^{-1}) with a 2 fs timestep. Five independent

simulations for each AC system were run. All bonds involving hydrogens were restrained using the SHAKE algorithm. Starting structures for QM/MM[38] modelling were chosen from MD simulations based on visual inspection of the active site hydration pattern and the 6α-hydroxyethyl orientation; this orientation was kept from changing during subsequent QM/MM US MD by applying a weak dihedral restraint (except in the case of orientation I). Free energy barriers for the first (rate-limiting) step of deacylation for the different active site conformations were determined from three separate QM/MM umbrella sampling (US) calculations for each conformation.[39] Two reaction coordinates were employed in US, one for the nucleophilic attack and one for the proton transfer, as in previous simulations of deacylation in serine β-lactamases.[35, 40-42] Sampling time in each window was 2 ps, and DFTB2 (SCC-DFTB)[43-45] was used as the QM method for regions consisting of 43 and 46 atoms (including link atoms) for imipenem and meropenem, respectively (Figure S1). Free energy surfaces (FESs) were constructed from 399 individual US windows. The weighted histogram analysis method (WHAM)[46, 47] was used to construct the free energy surfaces, and the minimum energy paths were analysed using the Minimum Energy Path Surface Analysis (MEPSA) program[48]. All simulations and trajectory analyses were done using the AMBER18 software package[49] (pmemd.cuda[50-52] for MM MD, and sander for QM/MM calculations).

Results & Discussion

Conformational Dynamics of Carbapenem:OXA-48 Acylenzymes

AC dynamics for both imipenem and meropenem complexed with OXA-48, each in the Δ2 (enamine) configuration, were explored by running five 200 ns MM MD simulations for each

complex. The first 50 ns were excluded from trajectory analysis to allow time for equilibration. For both carbapenems, the salt bridge between the C3 carboxylate and Arg250 was preserved during simulations, and the C7 carbonyl stayed in the oxyanion hole formed by the backbone amides of Ser70 (nucleophile) and Tyr211. The carbapenem C2 (tail) substituents sampled a range of conformations during the simulations, consistent with previous suggestions based on structural analysis.[29] Clustering the substrate poses based on their heavy atom RMSD yielded four distinct clusters per substrate, which differ by 0.8-1.8 Å and 1.7-2.5 Å for imipenem and meropenem, respectively, from the poses in the corresponding crystal structures (Figure S2, Table S1 and SI section Acylenzyme Clustering). The main deviations between cluster centroids and the crystal structure coordinates are due to the positions of the C2 tail groups, as the pyrroline ring and its substituents are anchored in place by hydrogen bonds to the oxyanion hole and the salt bridge with Arg250. However, for the crystal structures 6P97 and 6P98 there is only limited electron density beyond the sulfur atom for both imipenem and meropenem, so the deposited coordinates may not completely reliably depict the actual substrate binding poses. Additional clustering on the active site residues (explained in further detail in the SI) implies that there may be slight differences also in the positions of active site residues Lys73, Tyr157, as well as of the substrate (Figure S3 and Table S2).

During MM MD, the carbapenem 6α-hydroxyethyl group was able to rotate to occupy three different orientations, which can be distinguished by the value of the C7-C6-C-O dihedral angle: around 50°, 180°, or 290°, henceforth referred to as orientations I, II, and III, respectively (Figure 2). The 6α-hydroxyethyl orientation affects interactions in the active site, because its hydroxyl group can hydrogen bond either with the DW (I), or with the Lys73 carboxylate (III), or stay close to the crystallographically observed pose, in which its methyl group is positioned next to the DW

and points towards Leu158 (II, Figure 2). The starting orientation of the 6α-hydroxyethyl for both carbapenems is II, as in the crystal structures used in model construction. During MD simulations, this sidechain is free to move and sample all three orientations. For meropenem, orientation I is sampled more than II, while III is sampled only minimally (Figure 2). Conversely, both orientations II and III are sampled more than I for imipenem. The free energy difference between the different orientations of the 6α-hydroxyethyl group was estimated by calculating the ratio of MD trajectory frames corresponding to each orientation (Z), and using $\Delta G = RT\ln(Z)$, where R is the molar gas constant and T the simulation temperature (300 K). For imipenem, the lowest free energy state is orientation II, with slightly higher relative energies of 0.6 and 0.2 kcal/mol for orientations I and III, respectively. For meropenem, orientation I has the lowest free energy, orientation II is slightly higher (0.6 kcal/mol) but orientation III is significantly higher (2.2 kcal/mol). The presence of a methyl group in the 1β-position in meropenem (instead of a 1β-proton in imipenem) may explain the relatively higher penalty for orientation III, as in this orientation the 1β-substituent is located directly next to the 6α-hydroxyethyl moiety.

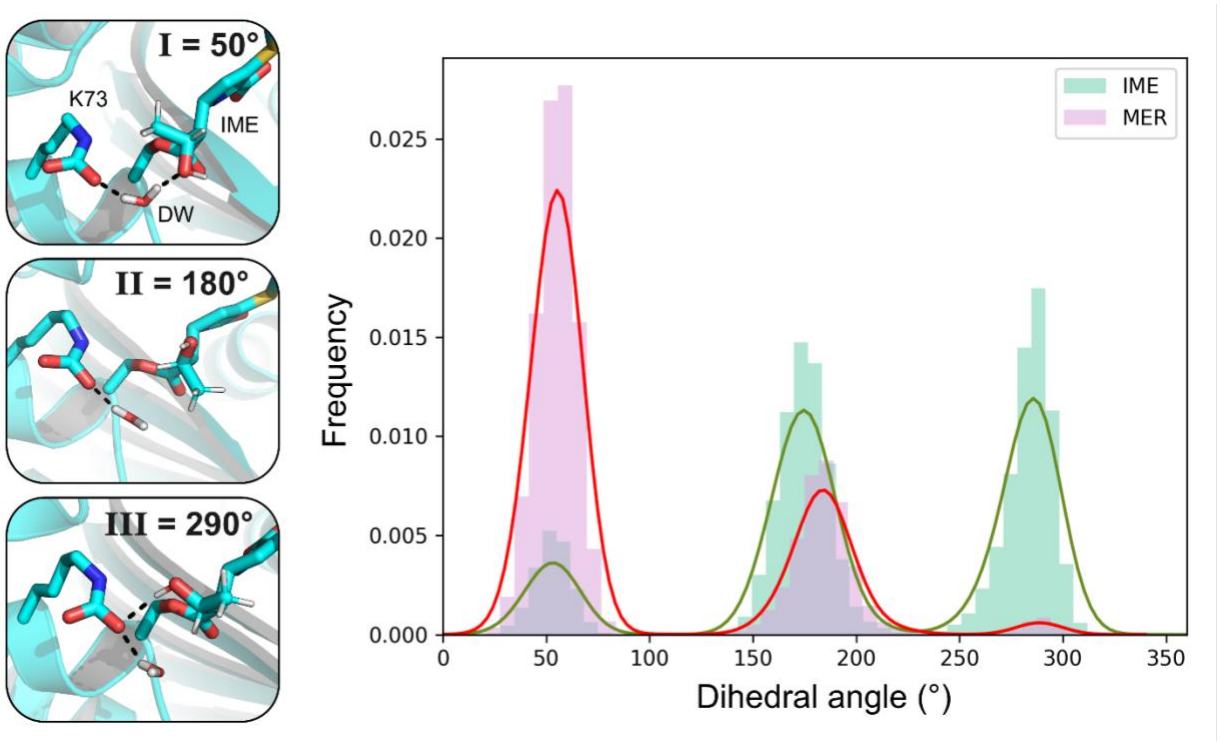

Figure 2. Conformational behaviour of the carbapenem 6α-hydroxyethyl group. Left: The 6α-hydroxyethyl group can assume three different orientations, which can be distinguished by the C7-C6-C-O dihedral angle values. When the dihedral is around 50° (orientation I), the hydroxyl group is hydrogen bonded with the DW, and in the 180° orientation (II) the hydroxyl group can only interact with solvent. In the 290° orientation (III), the hydroxyl group is donating a hydrogen bond to the carboxylated Lys73. Right: The distribution of sampled dihedral values during MM MD simulations of the imipenem (IME) and meropenem (MER) acylenzymes (5x150 ns per carbapenem).

Previously, our QM/MM simulations indicated that Leu158 may play an important role in modulating active site hydration in the deacylation of ceftazidime by OXA-48-like enzymes.[35] The orientation of Leu158 also differed initially between the two OXA-48/carbapenem systems, as the Cβ - Cγ bond has rotated by 180° in the meropenem structure. To study if Leu158 has a similar effect on carbapenem hydrolysis as observed for ceftazidime, its rotamers were first investigated by measuring the χ_1 dihedral (N-Cα-Cβ-Cγ) in MM MD simulations. The distribution of sampled rotamers is presented in Figure S4. After the heating phase, Leu158 essentially always rotates away from the crystallographic *g*- orientation ($\chi_1 \approx 290°$) to the *t* orientation ($\chi_1 \approx 180°$) to allow space for the 6α-hydroxyethyl moiety, which in turn also permits for two water molecules to form

hydrogen bonds with Lys73:OQ1. As the cephalosporin scaffold lacks a functional group similar to the 6α-hydroxyethyl group of carbapenems, typically bearing larger substituents in the β orientation at the equivalent 7-postion, it is likely that Leu158 does not possess a similar role in carbapenem hydrolysis to that suggested for cephalosporins.

Deacylation efficiencies for different orientations of the 6α-hydroxyethyl group

Because the interactions of the 6α-hydroxyethyl group in the active site have been suggested to play a role in modulating β-lactamase activity towards carbapenems,[32] deacylation free energy barriers were calculated separately for all three orientations of both imipenem and meropenem acylenzymes observed in MD simulations. Starting structures for US were chosen from the 200 ns MM MD simulations following two criteria: that a potential DW was at a suitable distance for nucleophilic attack, and the 6α-hydroxyethyl orientation was that desired. For orientations II and III, the sidechain dihedral was restrained close to the reference values to avoid the substrate changing between orientations during the reaction (no restraints were needed for I, as no sidechain rotation was observed during US). Overall barriers for deacylation were determined by combining sampling from three separate US calculations for each AC conformation (with different starting structures), with standard deviations calculated between the free energy barriers for individual US simulations (Table S3). More details of the US setup and analysis are available in the SI.

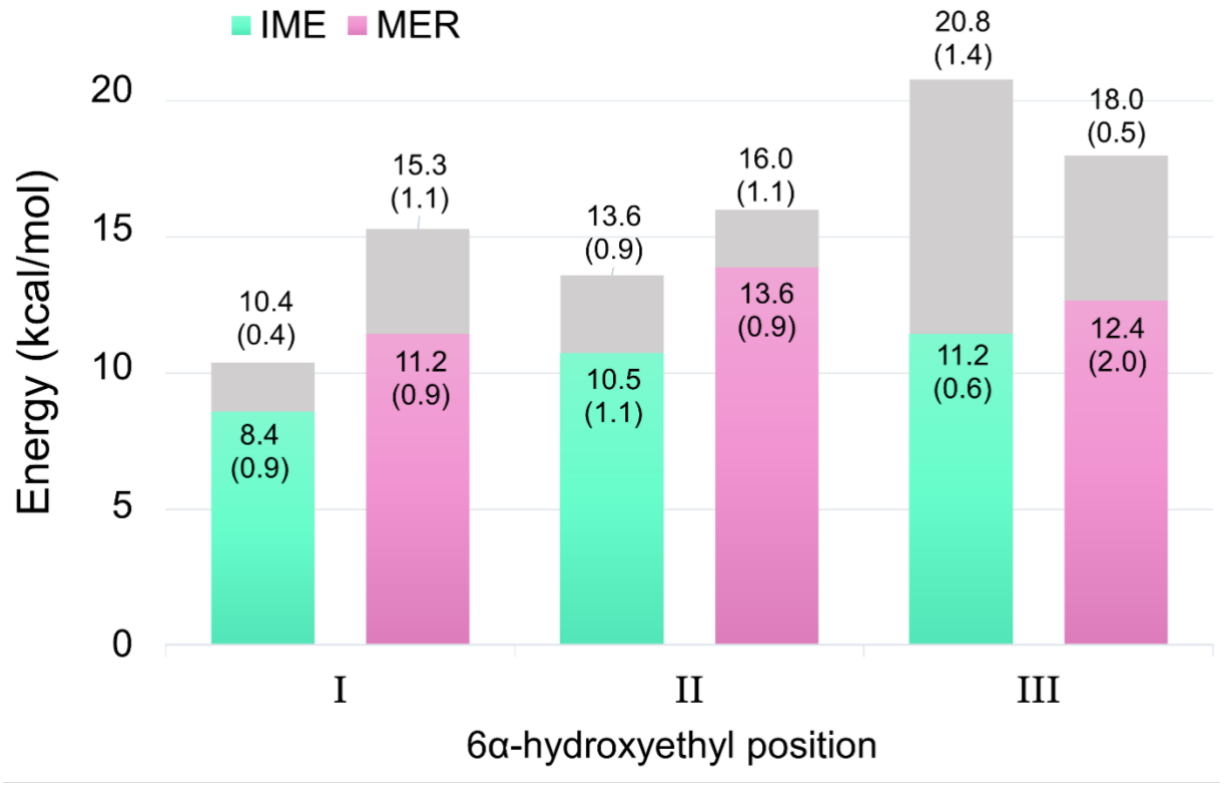

Figure 3. Free energy barriers for diacylation of carbapenem acylenzymes with the 6α-hydroxyethyl group in the three different orientations. Each bar includes the barrier obtained with a single water molecule hydrogen bonded to Lys73:OQ2 (lowest barrier, in colour; see Figure 4 for depiction of OQ2) and the barrier obtained with two water molecules hydrogen bonded to Lys73:OQ2 (highest barrier, in grey). Each barrier derived from three individual US simulations, standard deviations from the individual US calculations in parenthesis. Imipenem: green, meropenem: pink.

Figure 3 shows the calculated deacylation free energy barriers for the ACs formed by imipenem and meropenem with the three 6α-hydroxyethyl in each of the three orientations. For all orientations, two barriers are shown, which correspond to two different hydration states around the general base. The lower barrier (in colour) corresponds to a state with only one water molecule hydrogen bonded to Lys73:OQ2, and one or two waters hydrogen bonded to Lys73:OQ1 while the higher barrier corresponds to a state with two water molecules hydrogen bonded to both carboxylate oxygens (Figure 4, carboxylate oxygens labelled in Scheme 1). For all hydration

states, the calculated barriers follow the same trend of I < II < III, i.e. the lowest barriers are calculated for orientation I. Notably, the lowest barriers are consistently underestimated due to the QM method used (SCC-DFTB), as indicated by our benchmarking results (SI section "Benchmarking") and as is generally found for this method for similar reactions.[41, 42] Converting the experimentally determined k_{cat} values from one assay to free energy barriers using the Eyring equation gives activation free energies of 16.6 and 19.2 kcal/mol for imipenem and meropenem, respectively.[21] However, despite this difference between calculated barriers and those derived from experiment, we expect our protocol, using semi-empirical QM methods, to be a reliable indicator of relative energetic trends between different enzyme active site conformations, as we have demonstrated previously when studying deacylation of β-lactam acylenzymes of both by class A and D SBLs.[35, 42]

As discussed above and in ref. 35, increased hydration around the proton-accepting Lys73:OQ1 impairs deacylation in ceftazidime hydrolysis. A similar phenomenon was observed for carbapenems, with the additional observation that hydration around the second carboxylate oxygen (Lys73:OQ2) also affects reactivity. In orientation I, the average number of hydrogen bonds Lys73:OQ1 accepts during the reaction is 2.0-2.8 (calculated from the US minimum free energy path trajectories), which aligns with OQ1 being hydrogen bonded to two water molecules, and partly to Trp157. The two subpopulations with different deacylation barriers arise from a change in hydration around Lys73:OQ2. For the lower barriers in Figure 3, the number of hydrogen bonds to OQ2 is 1.3-1.5, and for the higher barriers 2.0-2.3 for orientation I. The lowest calculated deacylation barrier, 8.4 kcal/mol, is for imipenem in orientation I with one water molecule hydrogen bonded to OQ2 and two to OQ1 (Figure 4). The barrier increases by 2.0 kcal/mol when another solvent molecule donates a hydrogen bond to OQ2. For meropenem, the barrier is raised

by 4.1 kcal/mol upon introduction of an additional water molecule close to OQ2. The hydration effect around Lys73:OQ2 indicated here has an apparently smaller effect on the calculated barriers than that of hydration around Lys73:OQ1, since the presence of an additional water molecule hydrogen bonded to OQ1 raised the barrier for ceftazidime diacylation by approximately 5 kcal/mol.[35]

Orientation II (corresponding to a dihedral angle of between 147°-192° depending on the structure and protein chain) is observed in most OXA-48:carbapenem AC crystal structures. In this orientation, no part of the 6α-hydroxyethyl moiety interacts with either the DW or with Lys73, so the antibiotic may possibly not interfere with the reactive atoms. However, calculated deacylation barriers are increased by 2.1 kcal/mol for imipenem, and by 2.4 kcal/mol for meropenem, when comparing orientation II against I (in which only one water molecule is hydrogen bonded to OQ2). Having two water molecules donating hydrogen bonds to both OQ1 and OQ2 further raises the calculated barriers to 13.6 and 16.0 kcal/mol for imipenem and meropenem, respectively. Therefore, our simulations suggest that II is not the most deacylation-competent AC orientation. Additionally, orientation II might hinder the positioning of the DW in the active site in proximity to the electrophilic acyl carbon. For 93% and 87%, respectively, of the simulation times for the imipenem and meropenem acylenzymes in orientation II, the distance between the AC electrophilic carbon and the closest water molecule falls beyond 4 Å (an arbitrary threshold distance for a feasible nucleophilic attack; Figure S5). This is likely due to the 6α-hydroxyethyl methyl group partly occupying the space in the binding pocket for the deacylating water molecule, and thereby forcing this water further away from the AC. This is reflected in deposited crystal structures, as a DW candidate that is suitably positioned for nucleophilic attack is not observed in any OXA-48/carbapenem complex.[26-30] In a previous study (mainly based on

molecular dynamics), orientation II was observed to obstruct the positioning of the DW in the active site.[32] Docquier *et al.* concluded that only a slight repositioning of the methyl group of the 6α-hydroxyethyl sidechain is needed to better accommodate a water molecule at a suitable distance for nucleophilic attack. However, these conclusions are based on a single 10 ns MD simulation, which likely gives insufficient time to sample all available substrate orientations. Based on our MM MD simulations, as well as upon the calculated free energy barriers, orientation II is less likely to contribute to efficient deacylation of the carbapenem ACs. This is due both to an increase in energy required for deacylation, as well as to the lack active site configurations sampled, which would be suitable for the AC carbonyl to undergo nucleophilic attack by an incoming water molecule.

The largest increase in energetics between the two hydration states is calculated for orientation III, where the barriers increase by 9.6 and 5.6 kcal/mol for imipenem and meropenem, respectively, when the hydration state is changed. For the lower barriers, OQ1 and OQ2 form on average 1.9 - 2.1 and 1.4 - 1.5 hydrogen bonds, respectively, for the imipenem and meropenem complexes, while for the higher barriers the same numbers are 2.7 - 2.9 and 1.8 - 2.3 (data not shown). For the lower barriers, Leu158 has not (yet) rotated from the *g*- to the *t* rotamer (Figure S4), as the starting structures were chosen almost directly after the heating phase. The *g*- rotamer of Leu158 allows space only for the DW positioned near Lys73:OQ1, which was inserted into the active site in the starting model. Further, only one water molecule is donating a hydrogen bond to OQ2. Upon MD equilibration, Leu158 rotates, allowing for active site hydration to change to two water molecules hydrogen bonding to both carboxylate oxygens each. Subsequently, only the 'high barrier' hydration state is sampled. This explains the large increase in activation free energy when comparing the two hydration substates for orientation III, as two water molecules are added near

Lys73, as opposed to only one water molecule close to Lys73:OQ2 (as for orientations I and II). Therefore, our simulations indicate that III is the AC orientation that is the least competent for deacylation for the equilibrated system (in which Leu158 has rotated). Experimentally, this AC orientation is seen in the crystal structure of OXA-48 with hydrolysed, non-covalently bound imipenem (PDB ID 6PK0)[28], where the hydroxyethyl hydroxyl donates a hydrogen bond to the newly-formed carboxylate group. In our MM MD simulations of the AC, the exchange between 6α-hydroxyethyl dihedral orientations is frequent (indicating a low energy barrier). This is probably true also for the hydrolysed antibiotic, suggesting that rotation of this moiety can occur post-deacylation.

Further analysis of the US trajectories reveals that hydration around Lys73:OQ2 correlates with the rotamer of Val120. Valine has three rotamers for the χ_1 dihedral (N-Cα-Cβ-Cγ1): the *g*+ rotamer around 50°, *t* around 180°, and *g*- around 300° (Figure 4, Figure S6). In the starting structures for simulations, Val120 is in the *t* orientation for both carbapenems (for meropenem, partial occupancy for both *t* and *g*– rotamers was observed in the deposited structure, but only the *t* rotamer was used in the computational model building).[27] The rotameric state can switch to either *g*+ or *g*- during MD simulations (Figure S6). For the *g*+ rotamer, one of the methyl groups points directly towards Lys73, which only leaves space for a single water molecule next to Lys73:OQ2; this water is positioned to accept a hydrogen bond from Gln124 and to donate one to Lys73. Conversely, the *t* rotamer allows for a second water molecule to occupy the space between Lys73 and Val120, and this water molecule is able to donate hydrogen bonds to both Lys73:OQ2 and the Val120 backbone carbonyl. Val120 is part of motif II, which is formed by residues Ser118 - Val120 and is conserved across class D β-lactamases.[32] Together with Leu158, it forms the so-called 'deacylating water channel' in the vicinity of Lys73; this hydrophobic patch partly shields the

active site from bulk solvent.[27] For other OXA enzymes, a similar water channel has been proposed to open upon substrate binding to allow for water ingress into the active site and therefore for efficient deacylation.[53, 54] For OXA-48, previous comparison of apoenzyme and acylenzyme structures shows that substrate binding shifts Val120 and Leu158 only slightly, and that the water channel is more open than e.g. in OXA-23.[27] Access of water into the catalytic position next to the substrate and Lys73 is necessary for antibiotic hydrolysis, but as we indicate above, any additional solvent in the active site will impair reactivity. In OXA-48, it appears that Val120 (and the specific rotamers that it samples) is an important gateway residue controlling approach of bulk solvent to Lys73:OQ2. Our previous work (on ceftazidime hydrolysis in OXA-48-like enzymes) indicates that Leu158 modulates hydration around Lys73:OQ1.[35] Notably, Val120 is mutated to a leucine in OXA-519, a single point mutant of OXA-48; this mutation results in an increase in measured hydrolysis for some 1β-methyl carbapenems, such as meropenem and ertapenem, but decreased imipenemase activity. Compared to OXA-48, OXA-519 also increases the proportion of β-lactone reaction products, rather than conventionally formed ring-opened species, hydrolysis products of meropenem.[55]

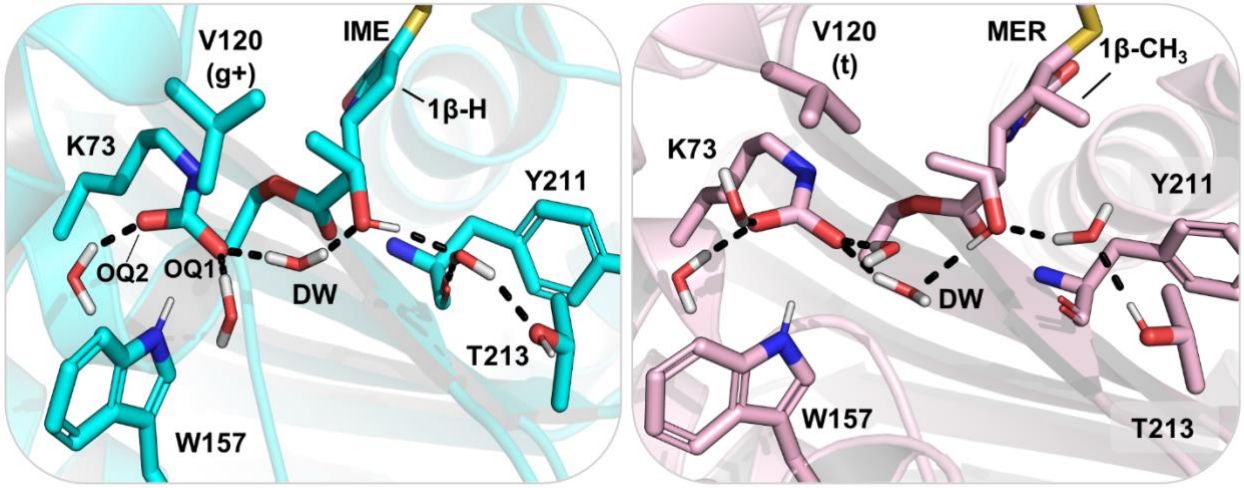

Figure 4. Alternative hydrogen bond configurations found with the 6α-hydroxyethyl in orientation I. Left: Active site of OXA-48 with imipenem in hydrogen bond configuration 1. Val120 adopts the g+ rotamer, and consequently only one water molecule is forming a hydrogen bond with Lys73:OQ2. The 6α-hydroxyethyl is in orientation I and donates a hydrogen bond to a water lodged between the Tyr211 backbone and Thr213. Right: Active site interactions of OXA-48 with meropenem in hydrogen bond configuration 2. Val120 is in its t rotameric state, which allows for two waters to hydrogen bond with both Lys73 carboxylate oxygens. The 6α-hydroxyethyl is in orientation I but donating a hydrogen bond to the DW.

Comparison of carbapenem deacylation in orientation I

As presented above, orientation I of the 6α-hydroxyethyl moiety is calculated to give the overall lowest deacylation free energy barriers for both carbapenems. The combined FESs for the hydration state with lower free energy barriers are presented in Figure S7 for all three substrate orientations. In this section, we focus further on orientation I and the 'reactive' active site configuration in which only one water molecule is hydrogen bonded to Lys73:OQ1, and two to Lys73:OQ2 (unless otherwise stated). For this AC conformation, two different hydrogen bonding arrangements in the active site are possible: the DW can donate a hydrogen bond to the 6α-hydroxyethyl hydroxyl group (named configuration 1), or the hydroxyl group can donate a hydrogen bond to the DW (configuration 2), see Figure 4. In MM MD, configuration (1) is sampled

for 87% and 86% of simulation time for imipenem and meropenem, respectively. In addition to donating a hydrogen bond to the DW as in (2), the 6α-hydroxyethyl hydroxyl group can also donate a hydrogen bond directly to Lys73:OQ1 if the DW is displaced. This orientation of the carbapenem 6α-hydroxyethyl group may be the relevant one for β-lactone formation, which has been characterised as a side product for OXA-48-catalysed carbapenem turnover, particularly of 1β-methyl carbapenems (such as meropenem).[55, 56] The β-lactone product has been proposed to form via intramolecular cyclisation, where the hydroxyl group acts as a nucleophile and donates a proton to Lys73. If the reaction occurs without a bridging water molecule, i.e. by a direct proton transfer between -OH and Lys73, lactonisation is most likely lower in energy in orientation I than in III, based on the trends observed for deacylation energetics.

For imipenem deacylation, both configurations (1) and (2) were observed in umbrella sampling. The lowest free energy barrier of 8.4 kcal/mol was calculated for configuration (1), and the barrier was increased by 2.0 kcal/mol for configuration (2). In addition to raising the free energy barriers, changing from (1) to (2) shifts the location of the transition state on the FES. For (1), the TS is located approximately at values –0.1 Å and 1.7 Å for the proton transfer and nucleophilic attack reaction coordinates, respectively. However, for (2), the TS location on the FES shifts to around –0.5 Å and 2.0 Å. Free energy surfaces with corresponding TS structures for both active site configurations are presented in Figure 5 and Figure S8. With active site configuration (2), the proton transfer has progressed further at the TS, whereas the approach of the DW oxygen to the acyl carbon is less advanced. This is potentially due to the additional hydrogen bond from the 6α-hydroxyethyl moiety hydroxyl decreasing the nucleophilicity of the DW, requiring the proton transfer reaction to have progressed further from the starting structure in the TS. Notably, a similar shift in the TS position on the FES is observed also in orientation III, where a water molecule is

donating a hydrogen bond to the DW instead of the 6α-hydroxyethyl group (Figure S7). Mulliken charge analysis of the key QM atoms does not reveal many significant differences for the calculated charges along the reaction when comparing US calculations with either configuration (1) or (2) (Tables S5-S8). The main difference is calculated at the TS, where for Lys73:OQ1, the charge is more positive and for DW:O the charge is more negative for configuration (2), as expected by the shift in the TS location towards the TI.

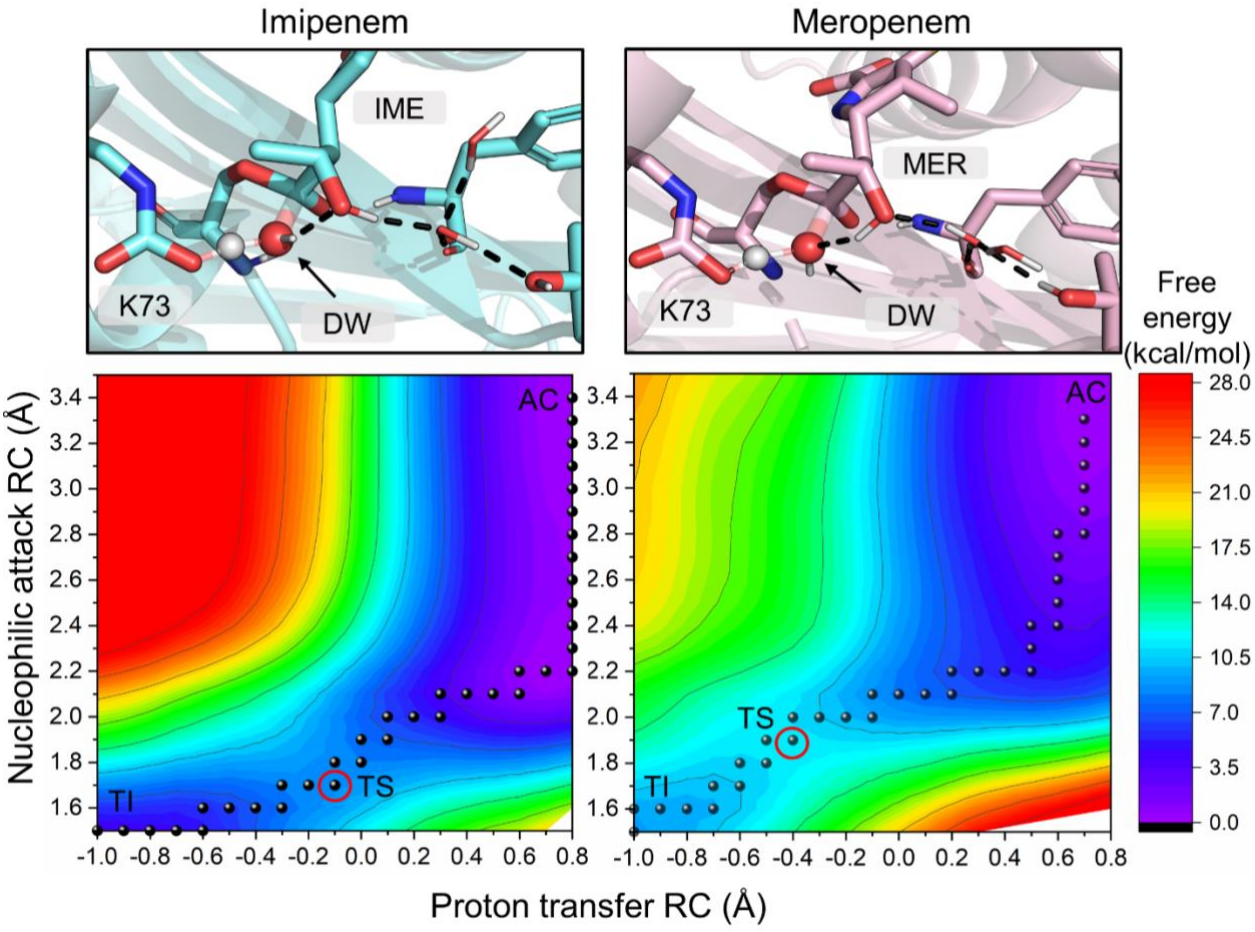

Figure 5. Free energy surfaces and transition state structures for alternative active site hydrogen bond configurations. Left: Free energy surface for imipenem deacylation for the lowest calculated barrier in orientation I (configuration 1). The DW is donating a hydrogen bond to the carbapenem hydroxyl group. Right: Free energy surface for meropenem deacylation with the lowest calculated barrier in orientation I (configuration 2). The carbapenem hydroxyl group donates a hydrogen bond to the DW. AC=acylenzyme, TS=transition state (marked by a red circle), TI=tetrahedral intermediate.

For meropenem, the lowest calculated deacylation barrier is 11.2 kcal/mol with an average of 2.4 and 1.4 hydrogen bonds accepted by K73:OQ1 and OQ2, respectively. This barrier is 2.8 kcal/mol higher than the lowest calculated barrier for imipenem, or 2.2 kcal/mol including the free energy penalty (derived from MM MD for imipenem) for orientation I. In contrast to imipenem, the hydroxyl of the 6α-hydroxyethyl moiety in meropenem always rotates during unrestrained US sampling to hydrogen bond configuration (2), donating a hydrogen bond to the DW. This rotation occurs before the TS is reached even when configuration (1) is present in the starting structure. Enforcing the donation of a hydrogen bond from DW to the 6α-hydroxyethyl -OH, i.e. restraining the reaction simulations to configuration (1), affects the location of the TS in a similar manner to that observed with imipenem. TS locations for configurations (1) and (2) are at –0.2/1.8 Å and –0.5/2.0 Å (proton transfer/nucleophilic attack), respectively. However, changing the hydrogen bonding pattern between configurations has only a minimal effect on the energetics, as the barrier for (1) is 11.9 kcal/mol. Therefore, the decrease in activation energy for configuration (1) vs. (2) does not follow the same trend for meropenem as it does for imipenem. Possible reasons for this may include the presence of a 1β-methyl group in meropenem, as this may hinder the rotation of the 6α-hydroxyethyl group to better optimise further hydrogen bonds between active site residues and water molecules nearby. A water molecule lodged between Tyr211 and Thr213 accepts a hydrogen bond from the carbapenem -OH moiety in configuration (1) or donates a hydrogen bond to it in configuration (2) (Figure 5 and Figure S8). The 1β-methyl group occupies the space above this water and may therefore induce its displacement or the re-organization of the surrounding water molecules to optimise hydrogen bonds between them, which could subsequently lead to a change from configuration (1) to (2). Additionally, the initial nucleophilic approach of the DW (from 3.5 Å to 2.2 Å) with the 6α-hydroxyethyl moiety in orientation I and hydrogen bond

configuration (1) is calculated to be slightly lower in energy for imipenem (Figure S9). Notably, the initial approach between the DW and the carbapenem is also slightly higher in energy in orientations II and III than in orientation I, which may contribute to their overall energetics being less favourable for deacylation. However, the reasons for the preference for the imipenem, but not the meropenem, complex to adopt configuration (1) are likely subtle and can result from small structural changes between the active site, substrate, and solvent molecules.

Comparison with experimental data

Most of the variants in the OXA-48 family are carbapenemases, with elevated imipenem hydrolysis rates when compared against other carbapenems.[57] For OXA-48, experimental measurements of k_{cat} values for imipenem hydrolysis vary between 1.5 and 22.5 s^{-1}, which can be converted to $\Delta^{\ddagger}G$ = 15.7 - 17.3 kcal/mol using the Eyring equation. For meropenem, the measured k_{cat} values range between 0.07 - 0.16 s^{-1}, which converts to $\Delta^{\ddagger}G$ = 18.7 - 19.2 kcal/mol. Using these figures as experimental estimates of free energies of activation, the difference ($\Delta\Delta^{\ddagger}G$) between imipenem and meropenem hydrolysis is between 1.4-3.5 kcal/mol, which is approximately the same magnitude as the strength of a single hydrogen bond (1-3 kcal/mol).[58] Hence, structural factors contributing to more efficient breakdown of imipenem, compared to 1β-methyl carbapenems, are most likely to be subtle. Our QM/MM simulations suggest that orientation I of the 6α-hydroxyethyl group is the most likely AC orientation to undergo deacylation, when this exists in a state with decreased hydration around Lys73:OQ2 (i.e., with only one water molecule donating a hydrogen bond to this carboxylate oxygen). When comparing the lowest free energy barriers calculated in orientation I for imipenem and meropenem (Figure 3), the difference for the

two substrates is $\Delta\Delta^{\ddagger}G$=2.8 kcal/mol; including the free energy penalty for the imipenem 6α-hydroxyethyl moiety adopting orientation I (0.6 kcal/mol, as determined from our MM MD simulations), the obtained $\Delta\Delta^{\ddagger}$G value drops to 2.2 kcal/mol. This is in excellent agreement with the experimentally determined range of $\Delta\Delta^{\ddagger}G$ values, which implies that the difference between imipenem and meropenem deacylation may indeed be caused by the subtle difference in the preferred hydrogen bonding patterns involving the DW and the 6α-hydroxyethyl sidechain reported here. In turn, the presence of the meropenem 1β-methyl group apparently contributes to this difference by influencing both the orientation of the 6α-hydroxyethyl group and the organization of water molecules in the near vicinity.

Overall, our analysis of the effects of active site conformations on carbapenem hydrolysis activity highlights the importance of controlling water access to the active site. On the one hand, it is crucial for the enzyme active site to support the binding of the deacylating water (through the aforementioned water channel). On the other hand, partial desolvation of the catalytic base (carboxylated Lys73) is required for efficient reaction. Such intricate control of active site solvation is a common feature of enzyme activity. For example, in ketosteroid isomerase, additional water molecules hydrogen bonding to the catalytic aspartate raise the barrier of reaction significantly.[59] Notably, this increased solvation occurs through water molecules hydrogen bonding to the carboxylate oxygen that is not receiving the proton, similar to what is observed here (difference between high and low barriers in Figure 3), but different from what we observed for ceftazidime hydrolysis. Such additional hydrogen bonding will decrease the pK_a of the catalytic carboxylate base,[60-62] weakening its proton affinity and thereby leading to higher barriers for the reaction. To avoid or limit the occurrence of additional hydrogen bonding to catalytic bases, enzymes have evolved active site architectures that can promote desolvation to increase

carboxylate reactivity. Such desolvation can for example be achieved by loop closure (as in triosephosphate isomerase and dihydrofolate reductase)[63, 64] or closure of the substrate binding cleft (as in ketosteroid synthase). Here, subtle control of the solvation around the carboxylated Lys73 is related to nearby hydrophobic residues (Val120 and Leu158), which can adopt conformations that allow the presence of the deacylating water but avoid more extensive solvation of the catalytic carboxylate.

Conclusions

We have modelled carbapenem hydrolysis by the OXA-48 β-lactamase using QM/MM reaction simulations. Deacylation reaction was modelled for two carbapenem substrates, imipenem and meropenem, to deduce the origin of the higher activity towards imipenem compared to other carbapenems. MM MD simulations of the acylenzyme complexes demonstrate that the carbapenem tail (C2) groups do not conform to any particular orientation but are able to adopt many different conformations. In contrast, the carbapenem 6α-hydroxyethyl group is able to rotate and to adopt three different orientations, where it either interacts with the DW (I), Lys73 (III), or is rotated so that the methyl group is oriented towards Leu158 (II). Subsequently, deacylation was modelled using QM/MM for both substrates in all of these three orientations to investigate the effect of orientation upon deacylation efficiency. Our calculated free energy barriers indicate that the most deacylation-competent orientation is I, where the hydroxyl group interacts with the DW, and that the orientation III has the highest free energy barriers.

Detailed comparison of the simulations revealed two factors that significantly affect the reaction energetics: hydration around Lys73, and the hydrogen bonding pattern between the DW and substrate, specifically the 6α-hydroxyethyl group. Hydration around the general base has been

proposed to affect the predicted hydrolysis rates for other β-lactam substrates;[35] here, we show that this is affected by hydration around both Lys73 carboxylate oxygens (not only the oxygen participating in proton transfer). Increased hydration around the non-reactive oxygen (Lys73:OQ2) correlates with higher calculated barriers; in turn, the orientation of Val120 correlates with the number of water molecules near this oxygen. Another aspect influencing deacylation efficiency is the pattern of hydrogen bonds in the active site that involve the DW and the carbapenem 6α-hydroxyethyl sidechain. Imipenem shows a preference for a configuration in which the DW donates hydrogen bonds to Lys73 and the 6α-hydroxyethyl hydroxyl group; the free energy barrier is higher when the hydroxyl group instead rotates to donate a hydrogen bond to the DW. This preference is not observed for meropenem, for which simulations with both hydrogen bond configurations have comparable energy barriers, which are similar to that calculated for imipenem in the less-favorable orientation. Therefore, we hypothesise that the difference between hydrolytic activities for the two carbapenem substrates stems from subtle differences in the active site hydrogen bonding patterns, which affect the reactivity of the DW. Furthermore, our results indicate that active site hydration is an important determinant of catalysis in OXA-48 enzymes: increasing hydration around the general base impairs carbapenem hydrolysis. Our study highlights the importance of detailed atomistic modelling in addition to experimental research to determine origins of catalytic activity, as simulation protocols such as those employed here can extend static crystallographic studies to enable investigation of the strength and dynamics of specific active site interactions during the catalytic cycle and directly investigate determinants of activity *in situ*.

ASSOCIATED CONTENT

Supporting Information. Further details concerning simulation set-up, analysis, and results are included in the Supporting Information.

AUTHOR INFORMATION

Corresponding Author

*Marc W. van der Kamp, marc.vanderkamp@bristol.ac.uk

Present Addresses

† Present address: Department of Biochemistry and Biophysics, Stockholm University, Svante Arrhenius väg 16, 10691 Stockholm, Sweden.

‡ Present address: Centre for Sport, Exercise and Life Sciences, Faculty of Health and Life Sciences, Coventry University, Coventry CV1 5FB, UK.

Author Contributions

The manuscript was written through contributions of all authors. VHAH and MWK designed the study, VHAH performed all simulations, assisted by TMW. All authors analysed the results, participated in writing the manuscript and have given their approval to the final version.

Funding Sources

VHAH and this research were supported by the UK Medical Research Council (MR/N0137941/1 for the GW4 Biomed DTP awarded to the Universities of Bath, Bristol, Cardiff and Exeter). MWK is a BBSRC David Phillips Fellow and thanks BBSRC for support (BB/M0626280/1). AJM thanks EPSRC for support (grant number EP/M013219/1). AJM and JS thank MRC for

funding (MR/T016035). This work was conducted using the computational facilities of the Advanced Computing Research Centre, University of Bristol.

ABBREVIATIONS

SBL, serine β-lactamase; MBL, metallo-β-lactamase; AC, acylenzyme; TS, transition state; TI, tetrahedral intermediate; QM/MM, quantum mechanics/molecular mechanics; US, umbrella sampling; FES, free energy surface

REFERENCES

1. WHO, Antibiotic Resistance, https://www.who.int/news-room/fact-sheets/detail/antibiotic-resistance, (accessed 01/19/2021).
2. V. M. D'Costa, C. E. King, L. Kalan, M. Morar, W. W. L. Sung, C. Schwarz, D. Froese, G. Zazula, F. Calmels, R. Debruyne, G. B. Golding, H. N. Poinar and G. D. Wright, *Nature*, 2011, **477**, 457-461.
3. J. Wang, P. Wang, X. Wang, Y. Zheng and Y. Xiao, *JAMA Intern. Med.*, 2014, **174**.
4. J. Davies and D. Davies, *Microbiol. Mol. Biol. Rev.*, 2010, **74**, 417-433.
5. *Review on Antimicrobial Resistance. Antimicrobial Resistance: Tackling a Crisis for the Health and Wealth of Nations.*, 2014.
6. S. L. Lammie and J. M. Hughes, *Annu. Rev. Food Sci. Technol.*, 2016, **7**, 287-312.
7. S. A. Ahmed, E. Barış, D. S. Go, H. Lofgren, I. Osorio-Rodarte and K. Thierfelder, *World Dev.*, 2018, **111**, 148-160.
8. L. L. Silver, *Clin. Microbiol. Rev.*, 2011, **24**, 71-109.
9. K. Lewis, *Cell*, 2020, **181**, 29-45.
10. S. Harbarth, U. Theuretzbacher and J. Hackett, *J. Antimicrob. Chemother.*, 2015, **70**, 1604-1607.
11. E. Y. Klein, T. P. Van Boeckel, E. M. Martinez, S. Pant, S. Gandra, S. A. Levin, H. Goossens and R. Laxminarayan, *Proc. Natl. Acad. Sci. U S A*, 2018, **115**, E3463-E3470.
12. *World Health Organization Model List of Essential Medicines, 21st List, 2019*, World Health Organization, Geneva, 2019.
13. E. Sauvage, F. Kerff, M. Terrak, J. A. Ayala and P. Charlier, *FEMS Microbiol. Rev.*, 2008, **32**, 234-258.
14. D. J. Tipper and J. L. Strominger, *Proc. Natl. Acad. Sci. U S A*, 1965, **54**, 1133-1141.
15. K. M. Papp-Wallace, A. Endimiani, M. A. Taracila and R. A. Bonomo, *Antimicrob. Agents Chemother.*, 2011, **55**, 4943-4960.
16. C. L. Tooke, P. Hinchliffe, E. C. Bragginton, C. K. Colenso, V. H. A. Hirvonen, Y. Takebayashi and J. Spencer, *J. Mol. Biol.*, 2019, **431**, 3472-3500.
17. R. P. Ambler, *Phil. Trans. R. Soc. Lond. B*, 1980, **289**, 321-331.

18. B. A. Evans and S. G. Amyes, *Clin. Microbiol. Rev.*, 2014, **27**, 241-263.
19. J. D. D. Pitout, G. Peirano, M. M. Kock, K. A. Strydom and Y. Matsumura, *Clin. Microbiol. Rev.*, 2019, **33**, e00102-00119.
20. K. S. Thomson and E. Munson, *J. Clin. Microbiol.*, 2017, **55**, 1608-1611.
21. S. Oueslati, P. Nordmann and L. Poirel, *J. Antimicrob. Chemother.*, 2015, **70**, 1059-1063.
22. L. Poirel, M. Castanheira, A. Carrer, C. P. Rodriguez, R. N. Jones, J. Smayevsky and P. Nordmann, *Antimicrob. Agents Chemother.*, 2011, **55**, 2546-2551.
23. F. De Luca, M. Benvenuti, F. Carboni, C. Pozzi, G. M. Rossolini, S. Mangani and J. D. Docquier, *Proc. Natl. Acad. Sci. U S A*, 2011, **108**, 18424-18429.
24. L. Dabos, A. Zavala, R. A. Bonnin, O. Beckstein, P. Retailleau, B. I. Iorga and T. Naas, *ACS Infect. Dis.*, 2020, **6**, 1032–1043.
25. S. Oueslati, P. Retailleau, L. Marchini, C. Berthault, L. Dortet, R. A. Bonnin, B. I. Iorga and T. Naas, *Antimicrob. Agents Chemother.*, 2020, **64**, e02329-02319.
26. S. Akhter, B. A. Lund, A. Ismael, M. Langer, J. Isaksson, T. Christopeit, H. S. Leiros and A. Bayer, *Eur. J. Med. Chem.*, 2018, **145**, 634-648.
27. C. A. Smith, N. K. Stewart, M. Toth and S. B. Vakulenko, *Antimicrob. Agents Chemother.*, 2019, **63**, e01202-01219.
28. A. Akhtar, O. A. Pemberton and Y. Chen, *ACS Infect. Dis.*, 2020, **6**, 261-271.
29. K. M. Papp-Wallace, V. Kumar, E. T. Zeiser, S. A. Becka and F. van den Akker, *Antibiotics (Basel)*, 2019, **8**, 145.
30. V. Stojanoski, L. Hu, B. Sankaran, F. Wang, P. Tao, B. V. V. Prasad and T. Palzkill, *ACS Infect. Dis.*, 2021, DOI: 10.1021/acsinfecdis.0c00798.
31. D. Golemi, L. Maveyraud, S. Vakulenko, J.-P. Samama and S. Mobashery, *Proc. Natl. Acad. Sci. U S A*, 2001, **98**, 14281-14285.
32. J. D. Docquier, V. Calderone, F. De Luca, M. Benvenuti, F. Giuliani, L. Bellucci, A. Tafi, P. Nordmann, M. Botta, G. M. Rossolini and S. Mangani, *Chem. Biol.*, 2009, **16**, 540-547.
33. F. Fonseca, E. I. Chudyk, M. W. van der Kamp, A. Correia, A. J. Mulholland and J. Spencer, *J. Am. Chem. Soc.*, 2012, **134**, 18275-18285.
34. C. T. Lohans, E. I. Freeman, E. V. Groesen, C. L. Tooke, P. Hinchliffe, J. Spencer, J. Brem and C. J. Schofield, *Sci. Rep.*, 2019, **9**, 13608.
35. V. H. A. Hirvonen, A. J. Mulholland, J. Spencer and M. W. van der Kamp, *ACS Catal.*, 2020, **10**, 6188-6196.
36. J. A. Maier, C. Martinez, K. Kasavajhala, L. Wickstrom, K. E. Hauser and C. Simmerling, *J. Chem. Theory Comput.*, 2015, **11**, 3696-3713.
37. E. Vanquelef, S. Simon, G. Marquant, E. Garcia, G. Klimerak, J. C. Delepine, P. Cieplak and F. Y. Dupradeau, *Nucleic Acids Res.*, 2011, **39**, W511-517.
38. J. Kästner, *WIREs Comput. Mol. Sci.*, 2011, **1**, 932-942.
39. R. C. Walker, M. F. Crowley and D. A. Case, *J. Comput. Chem.*, 2008, **29**, 1019-1031.
40. J. C. Hermann, L. Ridder, H. D. Holtje and A. J. Mulholland, *Org. Biomol. Chem.*, 2006, **4**, 206-210.
41. E. I. Chudyk, M. A. Limb, C. Jones, J. Spencer, M. W. van der Kamp and A. J. Mulholland, *Chem. Commun.* , 2014, **50**, 14736-14739.
42. V. H. A. Hirvonen, K. Hammond, E. I. Chudyk, M. A. L. Limb, J. Spencer, A. J. Mulholland and M. W. van der Kamp, *J. Chem. Inf. Model.*, 2019, **59**, 3365-3369.

43. G. d. M. Seabra, R. C. Walker, M. Elstner, D. A. Case and A. E. Roitberg, *J. Phys. Chem. A*, 2007, **111**, 5655-5664.
44. M. Elstner, D. Porezag, G. Jungnickel, M. Elsner, M. Haugk, T. H. Frauenheim, S. Suhai and G. Seifert, *Phys. Rev. B*, 1998, **58**, 7260-7268.
45. T. A. Niehaus, M. Elstner, T. H. Frauenheim and S. Suhai, *J. Mol. Struct. THEOCHEM*, 2001, **541**, 185-194.
46. S. Kumar, D. Bouzida, R. H. Swendsen, P. A. Kollman and J. M. Rosenberg, *J. Comput. Chem.*, 1992, **13**, 1011-1021.
47. A. Grossfield, WHAM: an Implementation of the Weighted Histogram Analysis Method, http://membrane.urmc.rochester.edu/content/wham/, (accessed 08/01/2020).
48. I. Marcos-Alcalde, J. Setoain, J. I. Mendieta-Moreno, J. Mendieta and P. Gomez-Puertas, *Bioinformatics*, 2015, **31**, 3853-3855.
49. D. A. Case, I. Y. Ben-Shalom, S. R. Brozell, D. S. Cerutti, T. E. I. Cheatham, V. W. D. Cruzeiro, T. A. Darden, R. E. Duke, D. Ghoreishi, G. Giambasu, T. J. Giese, H. Gilson, H. Gohlke, A. W. Goetz, D. Greene, R. Harris, N. Homeyer, Y. Huang, S. Izadi, A. Kovalenko, R. Krasny, T. Kurtzman , T. S. Lee, S. LeGrand, P. Li, C. Lin, J. Liu, T. Luchko, R. Luo, V. Man, D. Mermelstein, K. M. Merz, Y. Miao, G. Monard, C. Nguyen, H. Nguyen, A. Onufriev, F. Pan, R. Qi, D. R. Roe, A. Roitberg, C. Sagui, S. Schott-Verdugo, J. Shen, C. L. Simmerling, J. Smith, J. Swails, R. C. Walker, J. Wang, H. Wei, L. Wilson, R. M. Wolf, X. Wu, L. Xiao, Y. Xiong, Y. D. M. and K. P.A., *Journal*, 2019.
50. R. Salomon-Ferrer, A. W. Gotz, D. Poole, S. Le Grand and R. C. Walker, *J. Chem. Theory Comput.*, 2013, **9**, 3878-3888.
51. S. Le Grand, A. W. Götz and R. C. Walker, *Comput. Phys. Commun.*, 2013, **184**, 374-380.
52. R. Salomon-Ferrer, A. W. Götz, D. Poole, S. Le Grand and R. C. Walker, *J. Chem. Theory Comput.*, 2012, **8**, 1542-1555.
53. C. A. Smith, N. T. Antunes, N. K. Stewart, M. Toth, M. Kumarasiri, M. Chang, S. Mobashery and S. B. Vakulenko, *Chem. Biol.*, 2013, **20**, 1107-1115.
54. M. Toth, C. A. Smith, N. T. Antunes, N. K. Stewart, L. Maltz and S. B. Vakulenko, *Acta Crystallogr.*, 2017, **C73**, 692-701.
55. K. M. J. Aertker, H. T. H. Chan, C. T. Lohans and C. J. Schofield, *J. Biol. Chem.*, 2020, **295**, 16604-16613.
56. C. T. Lohans, E. van Groesen, K. Kumar, C. L. Tooke, J. Spencer, R. S. Paton, J. Brem and C. J. Schofield, *Angew. Chem. Int. Ed.* , 2018, **57**, 1282-1285.
57. V. H. A. Hirvonen, J. Spencer and M. W. van der Kamp, *Antimicrob. Agents Chemother.*, 2021, **65**, e00184-00121.
58. J. M. Berg, J. L. Tymoczko and L. Stryer, *Biochemistry. 5th edition.*, W. H. Freeman, New York, 2002.
59. M. W. van der Kamp, R. Chaudret and A. J. Mulholland, *FEBS J.*, 2013, **280**, 3120-3131.
60. S. Shan and D. Daniel Herschlag, *J. Am. Chem. Soc.*, 1996, **118**, 5515-5518.
61. M. A. Porter, J. R. Hall, J. C. Locke, J. H. Jensen and P. A. Molina, *Proteins*, 2006, **63**, 621-635.
62. L. Tao, J. Han and F. Tao, *J. Phys. Chem. A*, 2008, **112**, 775-782.
63. A. R. Mhashal, Y. Pshetitsky, C. M. Cheatum, A. Kohen and D. T. Major, *J. Am. Chem. Soc.*, 2018, **140**, 16650-16660.

64. Q. Liao, Y. Kulkarni, U. Sengupta, D. Petrovic, A. J. Mulholland, M. W. van der Kamp, B. Strodel and S. C. L. Kamerlin, *J. Am. Chem. Soc.*, 2018, **140**, 15889-15903.